Solid Earth Discuss., 6, 3261–3302, 2014
www.solid-earth-discuss.net/6/3261/2014/
doi:10.5194/sed-6-3261-2014

Solid Earth Discussions
Open Access

Syn-eruptive, soft-sediment deformation of dilute pyroclastic density current deposits: triggers from granular shear, dynamic pore pressure, ballistic impacts and shock waves

G. A. Douillet[1], B. Taisne[2], È. Tsang-Hin-Sun[3], S. K. Müller[4], U. Kueppers[1], and D. B. Dingwell[1]

[1]Earth and Environmental Sciences, Ludwig-Maximilians-Universität, Munich, Germany
[2]Volcano Group, Earth Observatory of Singapore
[3]Université of Brest and CNRS, Laboratoire Domaines Océaniques, Plouzaré, France
[4]Meteorological Institute, Ludwig-Maximilians-Universität, Munich, Germany

Received: 17 November 2014 – Accepted: 28 November 2014 – Published:
16 December 2014

Correspondence to: G. A. Douillet (g.douillet@min.uni-muenchen.de)

Published by Copernicus Publications on behalf of the European Geosciences Union.

Abstract

Soft-sediment deformation produces intriguing sedimentary structures and can occur in diverse environments and from a variety of triggers. From the observation of such structures and their interpretation in terms of trigger mechanisms, valuable information can be extracted about former conditions. Here we document examples of syn-eruptive deformation in dilute pyroclastic density current deposits. Outcrops from 6 different volcanoes have been compiled in order to provide a broad perspective on the variety of structures: Ubehebe craters (USA), Tungurahua (Ecuador), Soufrière Hills (Montserrat), Laacher See (Germany), Tower Hill and Purrumbete lake (both Australia).

Isolated slumps as well as sinking pseudonodules are driven by their excess weight and occur after deposition but penecontemporaneous to the eruption. Isolated, cm-scale, overturned beds with vortex forms have been interpreted to be the signature of shear instabilities occurring at the boundary of two granular media. They may represent the frozen record of granular, pseudo Kelvin–Helmholtz instabilities. Their recognition can be a diagnostic for flows with a granular basal boundary layer. The occurrence of degassing pipes together with basal intrusive dikes suggest fluidization during flow stages, and can facilitate the development of Kelvin–Helmholtz structures. The occurrence at the base of flow units of injection dikes in some outcrops compared with suction-driven local uplifts in others indicates the role of dynamic pore pressure. Variations of the latter are possibly related to local changes between depletive and accumulative dynamics of flows. Ballistic impacts can trigger unconventional sags producing local displacement or liquefaction. Based on the deformation depth, these can yield precise insights into depositional unit boundaries. Such impact structures may also be at the origin of some of the steep truncation planes visible at the base of the so-called "chute and pool" structures. Finally, the passage of shock waves emanating from the vent may be preserved in the form of trains of isolated, fine-grained overturned beds which may disturb the surface bedding without occurrence of a sedimentation phase in the vicinity of a vent.

SED
6, 3261–3302, 2014

Dilute pyroclastic density currents occur contemporaneously with seismogenic volcanic explosions. They are often deposited on steep slopes and can incorporate large amounts of water and gas in the sediment. They can experience extremely high sedimentation rates and may flow at the border between traction, granular and fluid-escape boundary zones. These are just some of the many possible triggers acting in a single environment, and reveal the potential for insights into the eruptive mechanisms of dilute pyroclastic density currents.

1 Introduction

The dynamics of pyroclastic density currents (PDCs) remain poorly understood. This is despite the fact that they are one of the most efficient transport means on the flanks of volcanoes exhibiting explosive eruptions, thereby yielding a major risk potential for life, environment and infrastructures. Analogue and numerical modeling approaches are well-suited to investigate targeted hypothesized processes, but the question of which process to model can only be answered through real PDC data. Cross-bedded, dilute PDC deposits can contain intriguing overturned and deformed patterns attributed to soft-sediment deformation (SSD). The understanding of these structures can yield insight into the syn- and post- depositional processes surrounding the bed interface: i.e. the basal boundary layer (BBL), the bed state, and conditions extant in the emplacement environment. In particular, syn-depositional SSD structures provide constrain on the shearing and dynamic pore pressure at the BBL that controls the sedimentation of PDCs, whereas syn-eruptive SSD records information on the eruptive dynamics and depositional units. PDCs are largely emplaced subaerially under metastable conditions favoring SSD. Thus a variety of specific SSD triggers may occur during an eruption and PDC deposits represent excellent targets for studies of SSD.

SED
6, 3261–3302, 2014

1.1 Soft-sediment deformation

Occasionally, stratified sediments exhibit anomalous patterns that cannot be explained by simple depositional schemes, and are understood as soft-sediment deformation (SSD) i.e. changes in the initial bed structure. This occurs during or shortly after deposition and prior to consequent diagenesis (Van Loon, 2009; Owen et al., 2011). SSD has been documented for subaqueous clastic sediments from the mud to coarse sand range (Van Loon, 2009), including subglacial environments (Ghienne, 2003; Denis et al., 2010; Douillet et al., 2012; Pisarska-Jamroży and Weckwerth, 2013), carbonates (Ettensohn et al., 2011; Chen and Lee, 2013), and volcanic ash (Gibert et al., 2011), but seems uncommon in subaerial settings.

A variety of triggers can be involved, predominantly related to seismogenic fluidization and/or liquefaction (special issue of Sedimentary Geology 235, Mohindra and Bagati, 1996; Owen, 1996), but also to tsunami waves (Alsop and Marco, 2012), storms (Chen and Lee, 2013) or volcanic base surges (Crowe and Fisher, 1973).

1.1.1 Nomenclature

There is neither a single classification scheme nor agreement on the nomenclature of SSD patterns (e.g., Lowe, 1975; Owen, 1987; Van Loon, 2009; Owen et al., 2011). Here, a non-generic nomenclature based on descriptive characteristics is employed:

Diapiric flame-like structures: laterally persistant deformation patches destroying the initial bedding. No coherent recumbence and dominantly vertical patterns (Crowe and Fisher, 1973; Owen, 1996; Niebling et al., 2010). They are distinguished from convolute/contorted bedding, the latter preserving the original bedset succession (Owen et al., 2011).

Pseudonodules and *dikes*: two layers of significantly different characteristics (densities, grain size) penetrate into each other, forming potatoids or small dikes (e.g., Mills, 1983; Owen, 2003; Owen and Moretti, 2008; Douillet et al., 2012). They can be de-

Discussion Paper | Discussion Paper | Discussion Paper | Discussion Paper |
SED
6, 3261–3302, 2014
Soft-sediment deformation of PDC deposits
G. A. Douillet et al.
Title Page
Abstract Introduction
Conclusions References
Tables Figures
Back Close
Full Screen / Esc
Printer-friendly Version
Interactive Discussion

tached from the layer to which they initially belong (Mills, 1983). Dikes are elongated and oriented quaquaversal to the layer they originate from.

Overturned laminae/beds: a few laminations or layers that show a coherent overturning recumbent towards the parent flow direction, laterally confined in otherwise undisturbed bedding. They can occur in sets of downstream repetitive but isolated patterns. They are distinguished from *overturned stratification*, which is an overturning of a stratal package as a whole (Allen and Banks, 1972; Røe and Hermansen, 2006; Bridge and Demicco, 2008, p. 357–358).

Vortex bedding: similar as overturned laminae, but with a vortex shape (Rowley et al., 2011). “Vorticity” is preferred to “rotation”, since any simple shear deformation includes a rotational component.

Folds-and-faults structures: repetitive folded beds with some angularity and discontinuities (microfaults) leading to concatenation (overlap). The general organization tends toward overturning with a coherent orientation (e.g., Odonne et al., 2011; Alsop and Marco, 2011).

The interpretation of the trigger mechanism(s) for SSD is not always straightforward and can include a combination of different effects. Here, distinction is made between the deformation, the agent of deformation, and the trigger. The deformation tensor in rock mechanics can be written as a sum of components of stretching, pure shear and simple shear (rotation). Identification of the relationships with the surroundings permits the interpretation of the physical agents responsible for the deformation as well as possible triggers.

Of interest here is the distinction between: (1) syn-sedimentary BBL (flow) shearing and dynamic pore pressure effects, (2) intra-deposit movements, and (3) post depositional mass movements. Bioturbation and biochemical effects are not dealt with here. BBL shearing includes the effects of the flow drag during or directly after sedimentation. It can be enhanced by the sediment state and the nature of the BBL. Intra-deposit movements lead to sediment fabric rearrangement and deformation. These are often related to the expelling of trapped fluids during or after sedimentation, in situ releases,

SED
6, 3261–3302, 2014

or compaction and loading. Mass movements are understood here as slumping, i.e. a short-scale, rather coherent sediment re-mobilization, the limit of which is taken to be debris flows. At the origin of the deformation can occur a trigger, a phenomenon that is not directly described in terms of the forces producing the deformation, but is causally responsible for their generation (e.g., ground-shaking facilitating fluidization of sediment, favoring fluid movements and producing pseudonodules).

1.2 PDCs and their possible SSD triggers

As particulate density currents, the depositional processes of PDCs are fundamental in their dynamics, since particles are both the agent of excess density driving momentum and the resulting sediment. Extreme and varied flow-substrate BBL processes may occur. The classification of Branney and Kokelaar (2002) emphasizes BBL processes and theorizes a classification into 4 types: granular-, fluid-escape-, fallout- and traction-dominated BBLs. Douillet et al. (2014) discussed different types of cross-bedding aggradation patterns as an upper or lower limit of the saltation threshold (the minimum shearing required to put grains in motion by wind), thus supposing a tractional BBL scheme. Alternatively, emplacement can be envisioned as a series of pulses with high basal concentration and no relationship to saltation, regardless of averaged concentration (Doronzo and Dellino, 2014), or stepwise *en-masse* deposition (Sulpizio and Dellino, 2008). The understanding of the nature and significance of BBL processes for PDCs may be further augmented by the study of syn-depositional SSD.

PDC deposits often display SSD (also "soft-state deformation", Branney and Kokelaar, 1994, 2002). This may be associated with subaqueous eruptions (Fiske, 1963) or subaqueous deposition (Brand and White, 2007; Brand and Clarke, 2009; Jordan et al., 2013), but also importantly, subaerial emplacement (Vazquez and Ort, 2006). Hot-state, plastic deformation including partial deformation of the clasts themselves is referred to as rheomorphism (Branney et al., 2004; Andrews and Branney, 2011). Lava flows may also deform underlying soft-sediment beds (Rawcliffe and Brown, 2014). The high sedimentation rate characteristics of particulate density currents re-

SED
6, 3261–3302, 2014

sults in metastable deposits prone to further re-arrangement (Smith and Kokelaar, 2013). Moreover, the variations from very fine to very coarse beds typical of pyroclastic deposits as well as common inverse grading make them susceptible to SSD after deposition (Gibert et al., 2011).

In addition to their metastable nature, the eruptive environment itself is subject to a variety of triggers. Seismic activity associated with eruption further destabilizes freshly emplaced pyroclasts. Syn-PDC processes can be recorded in SSD (Crowe and Fisher, 1973), and the likely formation of traction carpets and granular BBL can produce granular shear instabilities (Rowley, 2010; Rowley et al., 2011; Smith and Kokelaar, 2013). “Flame-like” structures are often reported (McDonough et al., 1984; Valentine et al., 1989; Brand and White, 2007; Brand and Clarke, 2009) and when interpreted as sheared structures, can serve to reconstruct palaeoflow directions (Giannetti and Luongo, 1994; Brown et al., 2008). Fluid escape SSD (dikes, pipes, plumes, pillars) can occur by escape of water accompanying phreatomagmatic eruptions (Nocita, 1988), degassing of fresh pyroclasts (Gernon et al., 2008, 2009), burning underlying vegetation, or be due to thermal expansion (Branney and Kokelaar, 2002, p. 61–66, and references therein). Interestingly, the high deposition rates combined with possible fluidized state of the flow can trap gases in the deposits that subsequently escape as degassing pipes within seconds after deposition (Komorowski et al., 2013). These can occur as fines-depleted pipes, few cms in length and diameter (Pistolesi et al., 2011; Smith and Kokelaar, 2013), or large dm to m scale depressions at the surface of deposits (Charbonnier and Gertisser, 2008). The high deposition rates also trigger simple load casts (Mattsson and Tripoli, 2011). Blocks ejected ballistically during an eruptive event deform the fresh deposits by landing (Gençalioğlu-Kuşcu et al., 2007; Jordan et al., 2013). Post eruptive processes are also common on steep sided volcanic edifices, with freshly deposited material likely to be unstable and slump (Fiske and Tobisch, 1978; Voight et al., 1983; Branney and Kokelaar, 1994; Ward and Day, 2006) as well as inherent contraction and compaction fractures following emplacement (Whelley et al., 2012).

SED
6, 3261–3302, 2014

1.3 Granular shear instabilities

Observations of syn-flow shear structures bring further insights into the BBL processes of PDCs. Simple shear is often invoked for the formation of overturned stratification (e.g., Allen and Banks, 1972; Mills, 1983; Røe and Hermansen, 2006). For such structures, the flow transmits and imposes part of its shear stress to the ground and thus translates the uppermost beds. In the other hand, sheat instabilities can be produced at the boundary between two fluids to form recurrent, vortex-shaped, Kelvin–Helmholtz instabilities. Valentine et al. (1989) suggested that flame-like SSD structures could be related to Kelvin–Helmholtz instabilities "between the bedload fluid and the overlying surge". Several analogue experimental studies with granular flows over grain beds have evidenced isolated but recurrent wave-like instabilities at the bed-flow interface (Goldfarb et al., 2002; Mangeney et al., 2010; Rowley, 2010; Roche et al., 2013; Farin et al., 2014). Goldfarb et al. (2002) have produced trains of wave instabilities with the shape of overturned laminae and noted that those were "likely produced by shearing differences" and "lacked any kind of vorticity". However, a rotational component must be present to produce the observed shark fin patterns. Rowley (2010) and Rowley et al. (2011) have imaged trains of shear-instabilities with well-developed vortex bedding convincingly interpreted as granular Kelvin–Helmholz instabilities. They further demonstrate the periodicity of these structures and document field examples. The wavy nature of those instabilities was further demonstrated in Farin et al. (2014), which also noted that the wavelength and amplitude are greatest for slopes close to the repose angle (highest speed). Roche et al. (2013) provided videos of the instabilities and an explanation for the fluid-like behavior of these instabilities. They suggested as a mechanism that negative dynamic pore pressures fluidize fine-grained beds and deform them as a whole rather than as individual grains. Other experimental work with granular flows has evidenced intriguing inter-penetration of beds over sinusoidal surfaces (Caicedo-Carvajal et al., 2006), longitudinal vortices in the flow direction (Forterre and Pouliquen, 2001), or Taylor vortices (Conway et al., 2004).

SED
6, 3261–3302, 2014

2 Geological settings and data

The SSD structures presented here belong to different volcanoes and both magmatic and phreatomagmatic eruptions of various intensities and depositional environments. As pointed by Mills (1983), SSD should be studied within their environment, and thus a brief context is introduced. Several types of SSD are identified with orders of magnitude between their dimensions as well as between the grain size of layers involved. Description of all discussed SSD structures is presented in Table 1.

2.1 Ubehebe crater (California, USA)

Ubehebe tuff ring is part of the Holocene/Pleistocene Ubehebe Craters complex and may have erupted between 0.8–2.1 ka (Sasnett et al., 2012). They erupted onto ancient lake sediments, at least partially phreatomagmatically. The arid climate does not explain the phreatomagmatic activity and interaction with a shallow water table is preferred (Sasnett et al., 2012). Crowe and Fisher (1973) reported SSD structures such as: contorted beds without preferred orientation, flame structures oriented with the flow direction and disrupted layers of thin tuff curled and pulled apart. They mapped the orientation of ballistic impact sags, mention post-eruption slumping on the Northwestern and Southeastern parts of the crater, and noted that SSD occurs within pre-existing channels filled with massive deposits but is absent in cross-bedded dominated overbanks. Here, a variety of SSD structures are documented from the Southern flank: folds-and-faults, curled layers, ballistic impact sags, a diapiric flame-like horizon and vortex features (Fig. 1).

2.2 Tungurahua (Ecuador)

The 17 August 2006 PDCs (Kelfoun et al., 2009; Hall et al., 2013; Bernard et al., 2014) are not linked to phreatomagmatic processes but rather to accumulation and subsequent destabilization of pyroclasts near the crater. The overbank sediments containing

SED
6, 3261–3302, 2014

the SSD structures have been interpreted to have formed from dilute PDCs originating from dense PDCs by flow stripping (Douillet et al., 2013b). SSD was identified in a lacquer peel within well-developed mm-scale ash lamination (Fig. 2) located on the lee side (approx. 20 cm from the crest) of an aggrading, transverse dune bedform that indicated very high sedimentation rates (Douillet et al., 2013a) approx. 6 km from the vent. Two clusters of small-scale overturned and recumbent laminae occur at different height in the same horizons. The upper structure exhibits a single, well developed overturned laminaset (Fig. 2b), whereas the lower one is a cluster of several recumbent anticlines followed by relatively massive material with diffuse oversteepened bedding in the upstream direction (Fig. 2c and d).

2.3 Soufrière Hills (Montserrat)

The 11 February 2010 partial dome-collapse event of Soufrière Hills (Montserrat) produced a series of 6 block and ash flows, 5 of them occurring within 15 min and was the largest event since the 1995 awakening (Wadge et al., 2014; Stinton et al., 2014). Numerous degassing pipes were observed in block and ash flow deposits as well as massive ash units (Stinton et al., 2014). Other post-depositional structures are described by Stinton et al. (2014) as "rootless phreatic explosion craters", textiti.e. structures related to hot blocks turning water into steam explosively. They can have diameters between 1 and 30 m, consist of "decimetre-sized blocks in a coarse ash-rich matrix derived from the underlying primary PDC deposits" and have a contact to underlying cross-bedded units or down to the pre-collapse surface. Here, SSD structures are documented from the Belham river valley less than 6 km from the vent (Fig. 3). According to Stinton et al. (2014), only three PDCs flowed in this drainage (stage 3-H, 4-K and 4-6), Wadge et al. (2014) also mentioning PDCs in this zone for the 11 February 2010 collapse. Basal, small-scale dikes and pseudonodules intrude in underlying diffusely cross-stratified ash from a massive lapilli and ash lens, whereas fines-poor, small-scale pipes are found in the otherwise ash-rich, massive, overlying layer (Fig. 3a and b). The top of the latter has a contact with a series of 3 vortex and undulating forms (Fig. 3b). These deposits

SED
6, 3261–3302, 2014

are found in the thalweg of the river valley, which may have contained some water. Another outcrop exhibits a large scale circular depression (ca. 3 m diam.) with ca. 10 cm deflation at the surface of the deposits (Fig. 3c).

2.4 Laacher See (Germany)

Laacher See was the location of a large eruption commonly attributed to phreatomagmatic explosions around 11 800 yr B.P. (Schmincke et al., 1973). Dune bedforms cross-stratification made of coarse lapilli to fine ash intercalated with lapilli to volcanic dust fall horizons occur over tens of km^2. Three isolated SSD structures are found around the "Wingertsbergwand" area, several km southward from the inferred vents (Fig. 4). A composite SSD structure several m long and ca. 1 m thick occurs as a lateral series of tilted blocks that evolve into folds-and-faults beds in the (approximate) downstream direction, accommodating a local compression (Fig. 4a–f). It is abruptly confined in depth by the lower ash layer and underlying beds show no sign of deformation. A few tens of m distant, a structure of similar dimensions characterized by oversteepened lamination and downward oriented, massive, lapilli pseudonodules resembles a "chute and pool" structure (Fig. 4g–i). A further structure approx. 150 m away, has a convex symmetrical form (ca. 10 cm vertical displacement) in an initially planar fine-grained bed. It is intercalated above a massive ash bed and below coarse-ash to lapilli, sub-planar, diffuse bedsets (Fig. 4j and k). Flow direction inferred from overlying cross-beds is roughly oriented from left to right but may be sub-parallel to the outcrop wall. The bed is partly missing on the right from the deformation. Similar ash layers pinch out above the convex shape and may represent an overlap of the same unit.

2.5 Tower Hill (Victoria, Australia)

Tower Hill maar (ca. 35 000 yr B.P., Sherwood et al., 2004; Prata and Cas, 2012) exhibits intriguing trains of oversteepened laminations contained within a single bedset (Fig. 5). They outcrop in the upper part of the southern rim (CRB quarry), parallel to the

SED
6, 3261–3302, 2014

crater wall. Underlying beds fine up from massive coarse ash and lapilli by increasing occurrence of thin, sub-planar, ash beds forming a diffusely stratified lapilli-ash facies. This grades into the fine-grained ripple beds with topping SSD and the reverse sequence occurs above. This sequence suggests a fall phase progressively influenced by pseudo base-surge (in the sense of Waters and Fisher, 1971) with increasingly efficient fragmentation related to phreatomagmatic explosions at the fine-grained SSD bedsets (optimally efficient water : magma ratio in Prata, 2012). The flow direction inferred from the underlying ripple bedding is oriented roughly parallel to the lateral extension of the outcrop (Prata, 2012). The SSD consists of isolated, oversteepened laminations with coherent orientation. They are recurrent with wavelength of ca. 50 cm and over hundreds of m.

2.6 Purrumbete Lake (Victoria, Australia)

The deposits forming the Purrumbete maar (ca. 20 000 yr B.P.) are characterized by three temporally separated eruption phases and vent locations, with relatively dry as well as wet phreatomagmatic conditions (Jordan et al., 2013). Ballistic bombs with impact sags are widespread in these deposits, suggesting wet deposits (Jordan et al., 2013). The SSD documented here outcrops with two faces at right angles. Perpendicular to the crater, folds-and-faults structures increase in size, faulting and recumbence outward from the vent (Fig. 6a, b and e), but parallel to the rim, only chaotic flame-like structures are visible (Fig. 6c and d). The overlying deposits are planar laminated ash with individual laminae followed over several m. They lie conformably on the SSD horizon and are related to fallout.

3 Discussion and interpretation

As a general observation, many of the examples documented have a fine-grained underlying or basal layer (Purrumbete, Laacher See, Ubehebe, Merapi). Fine-grained layers are likely to have distinct rheological properties which yield the onset of deformation (Mills, 1983). Ash is no exemption, at both small (Gibert et al., 2011) and regional scales (Wiemer, 2014, and references therein). Fine deposits are likely to have low permeability, impacting either on the transfer and diffusion of dynamic pore pressure from subsequent flows (Roche et al., 2013), or on fluid escapes from enclosed layers (Peltier et al., 2012).

3.1 Deformation driven by gravity

3.1.1 Slumps

For the Ubehebe thrusting folds-and-faults (Fig. 1a, top), observations point toward a gravitational slump: (1) deformed beds confined between undeformed strata, (2) large number of beds involved, (3) overturn orientation toward the thalweg of a channel, (4) axial planes of folds dipping upslope with folds' strike normal to microfaults, (5) imbrications and overlap (stacking) of deformed layers. The base of the folds-and-faults (Fig. 1a, base, and 1c) shows components of rotation, mixing and layer pull apart, indicating the floor thrust of slumping. Given the coherent state of the beds involved combined with their great variations in grain size and the thickness of SSD, a subaerial slump of wet sediment is favored. This would enhance cohesion and explain the gravity-sliding by overweight due to water. The interpretation is further supported by the characteristics of the nearby ballistic impact sags. Overlying strata are not deformed and so the slump has occurred during or between eruptive phases.

3.1.2 Granular Rayleigh–Taylor instabilities

The diapiric flame-like structures at Ubehebe (Fig. 1d) are remarkably similar to structures produced by granular Rayleigh–Taylor instabilities between a granular medium and air (Niebling et al., 2010). Usual interpretations of such features point toward liquefaction, loading, or water escape structures (e.g., Owen, 1996), a situation prone to

SED
6, 3261–3302, 2014
Soft-sediment deformation of PDC deposits
G. A. Douillet et al.

occur during the eruption with high sedimentation rate and wet deposits. These explanations correspond to forms of granular Rayleigh–Taylor instabilities (Selker, 1993; Vinningland et al., 2007, 2010). Some of the flame-like structures are overturned toward the flow direction, which may indicate shearing and syn-PDC SSD.

The curled and pulled apart, coarse-grained, isolated, flat "pseudonodules" from Ubehebe (Fig. 1b) are interpreted as detached load casts. These form in the presence of an inverse density gradient resulting from changes of porosity driven by the grain size distribution of successive layers (Mills, 1983; Bridge and Demicco, 2008, p. 353–354). As such, these also share the configuration for granular Rayleigh–Taylor instabilities. A shock (seismicity or impact) may trigger detachment, but is not necessary, and those structures may be post-eruptive. Their localized nature is taken to rule out remote triggers such as seismicity and no subsequent impact is visible above the structures. Further dynamic considerations coupled with the pseudo-wavelength of the structures and interface characteristics may resolve the question of their similarity with Rayleigh–Taylor instabilities (see Selker, 1993, and Appendix).

3.2 Deformation driven by shearing of subsequent flows

3.2.1 Granular shear and pseudo-Kelvin–Helmholz instabilities

At Tungurahua, the imbrication of overturned laminae with confinement within an otherwise undeformed bedset suggests syn-depositional processes (Fig. 2). SSD cannot be correlated with any impact sag. The orientation parallel to the flow direction suggests the influence of the latter. The vortex-shaped SSD structures are interpreted as granular shear instabilities related to Kelvin–Helmholtz vortices, based on reports and interpretations from analogue experiments (Rowley et al., 2011; Farin et al., 2014). If a pure wind BBL had moved the sediments, they would have begun to saltate as individual grains rather than deform as a whole (Douillet et al., 2014), and since the deposits were dry, no water can have triggered cohesion. Roche et al. (2013) explains the formation of wave instabilities at the interface between a fine-grained erodible bed and granular flow as linked with movements as a whole related to fluidization. This suggests that the observed features are indicative of a granular BBL and possible occurrence of traction carpets on the lee of the dune bedform. Although cross-stratification is generally interpreted as indicative of low particle concentration at the BBL, experiments by Leclair and Arnott (2005) have shown that laminations can be produced at more than 35 % particle concentration, a concentration at which a granular BBL can occur. The scale of the structures being similar to experimental results, the granular BBL is interpreted to be of the same order of thickness and velocities (few cm thick and few $m\,s^{-1}$ velocity).

The downflow evolution of SSD at Tungurahua (Fig. 2c and d) brings further support to the discussion of Rowley et al. (2011). Indeed, they suggested that pseudo Kelvin–Helmholtz vortices may only be anecdotal in sedimentary records, since they intrinsically mix the deposits and create graded massive units. In the outcrop, well defined and thin lamination is visible downstream of the deformation front highlighted by vortices. In contrast, upstream from the front, stratification is comparatively thick and massive, with diffuse oversteepened laminations contained within the layers (Fig. 2d). This indicates the ploughing effect of the downstream migrating vortices that tend to mix and homogenize the initial bedding, as predicted by Rowley et al. (2011).

The recumbent and vortex structures at Ubehebe (Fig. 1d) have an overturning orientation with flow and a vortex shape. They only differ from Tungurahua by their occurrence in otherwise massive deposits. This may be an effect of successive ploughing by Kelvin–Helmholtz vortices or simply result from massive deposition. A vortex form is also observed at Soufrière Hills (Fig. 3b, top). In this case, the vortex is followed downstream by a gentle undulation and a steep step. Although the second and third structures have not a vortex shape, they are interpreted as proto, granular Kelvin–Helmholtz instabilities at different development stages, and the downstream repetition of deformation is taken as sign of the wavy nature of the instability.

Interestingly, sheared structure with a vortex-like structure are also present on the stoss and crest of dune bedforms covered by aggrading bedsets at Roccamonfina

SED
6, 3261–3302, 2014

volcano (Italy, Fig. 5 in Giannetti and Luongo, 1994). If all these structures represent granular Kelvin–Helmholtz instabilities, they could share similar dynamics to their fluid analogue and quantitative information could be derived (Rowley et al., 2011, developed in Appendix). From theoretical considerations, BBL velocities of more than 2.5 $m\,s^{-1}$ for 1 % relative particle concentration are necessary for instabilities to develop (Appendix, Fig. 8). This number rapidly drops for higher flow concentrations, and shear instabilities thus plausibly develop for basal granular BBL few cm in thickness.

3.2.2 Influence of dynamic pore pressure

SSDs from Soufrière Hills seem to originate from the dark mLA lensoidal layer that connects to the small basal dikes and intrusions and to the overlying pseudonodules and pipes (Fig. 3a and b). Komorowski et al. (2013) interpret small degassing pipes in the deposits of the Merapi 2010 block and ash flows as related to rapidly deposited and fluidized flows. Here, the dark mLA layer is interpreted as fluidized and overpressurized in dynamic pore pressure during flow in order to explain the basal dikes and intrusions as injection features. Basal dikes in subglacial deposits are indeed usually interpreted as indicating overpressure of the flows and injections (e.g., Douillet et al., 2012). The associated mLA layer would have held part of the overpressure through rapid sedimentation, and subsequently released the gas during deflation and compaction after burial by the overlying layer. This could further have destabilized the overlying beds and eased the formation of shear instabilities found at the upper interface of the mA layer above the pipes. Alternatively, the influence of bed water turned into steam cannot be ruled out in the river thalweg. The large scale depletion of the surface (Fig. 3c) may relate to similar deflation of fluidized pockets, although simple re-arrangement of the grains underneath or any depletion could lead to similar surface expressions. The surface mainly consists of coarse particles and small deflation cracks developed, thus the structure may relate to fines' elutriation. A relation with the "phreatic rootless explosions" in Stinton et al. (2014) is not favored.

SED
6, 3261–3302, 2014

The convex deformation of the fine-grained planar strata at Laacher See (Fig. 4j and k) lacks any recumbent component, is isolated and no impact is visible. A localized decrease of the dynamic pore pressure of subsequent flows may have been transferred to the ground and slightly deformed the fine bed by suction. The deformed layer would have acted as a comparatively impermeable seal, containing the underpressure above it and lifting up. Negative dynamic pore pressures are indeed recorded from experimental granular flows and PDCs and trigger remobilization (Roche et al., 2013; Farin et al., 2014; Bernard et al., 2014). The dune bedform found just above the SSD may also have had some influence and produced a slight overweight. Aeolian dunes produce SSD on underlying beds, yet rather as load structures and in static settings (Chan and Bruhn, 2014).

The influence of dynamic pore pressure in destabilizing the sediment bed may be of importance in all syn-flow SSD scenarios. Both over- or under-pressurization can occur, and may connect with a flow's inhomogeneity. An overpressure is usually associated with flow front, and is directly followed by underpressure. Overpressurization may also be linked with accumulative flows, whereas underpressure relate to depletive evolution.

3.3 Deformation driven by ballistic impacts

3.3.1 Impact records

At Laacher See, the tilted blocks (or domino/bookshelf structures) and thrust folds-and-faults packages locally share characteristics with slump folds (Fig. 4a–f). However, the very limited throw, absence of significant slope or possible slump trigger and the nested nature appear to exclude this interpretation. Given the great thickness of the disturbed beds, a surface instability, simple shearing or granular Kelvin–Helmholtz instability, also seems unlikely.

Yet, there is a preferential orientation directed roughly outward from the postulated crater. The lateral evolution of the SSD leads another insight. (1) The upstream part

SED
6, 3261–3302, 2014

dominated by tilted blocks indicates extension (Fig. 4a and d). (2) The central part with the concave shape of the upper beds together with upward-penetrating flame-like beds suggest vertical compression (Fig. 4b and e). (3) The folds-and-faults and local decollement in the downstream part record lateral displacement away from the central part ("escape zone", Fig. 4c and f). The source of the SSD can thus be localized above the central part, in the vertical compression zone, and have forced local displacement to the right. In light of this, the SSD is interpreted as the print of a large block bouncing on the bed and transmitting a deformation oriented with its trajectory. This is further supported by the presence of large blocks (> 3 m diam.) in nearby areas in deposits otherwise dominated by ash and lapilli. Noteworthy, the abrupt confinement of the deformation in depth indicates a higher state of compaction of the undeformed beds, and thus their belonging to an older event separated by sufficiently long time for compaction. The basal ash layer would represent an initial fall event belonging to the deformed unit. Thus impact sags may also be used to trace genetic units.

The diagnosis is easier at Ubehebe (Fig. 1e), where impacting blocks are nested in deformed beds and just above pseudonodules and dikes. Thorough observation indicates that the coarse and massive layer escaped into the enclosing fine-grained beds: it is the most disturbed and exhibits pseudonodules and small dikes with respect to both the over and underlying layers, which still contain stratification. The isotropic nature of the leakage with apparent absence of preferential escape directions supports a liquefaction mechanism. To account for the coarse-grained nature, water saturation is inferred, in agreement with the other Ubehebe SSD structures. A grain-flow triggered by an impact-induced liquefaction of the porous and water saturated coarse-ash enclosed in impermeable fine-grained layers has likely produced the nodules and dikes.

The pseudo "chute-and-pool" from Laacher See (Fig. 4g–i) shares similarities with both impact structures. The central part exhibits a depression with concave beds indicating compression. The right part is disturbed by massive lapilli material with downward-oriented pillows/pseudonodules (mL and PN in Fig. 4h and i). These are related to a liquefied grain flow of porous and water saturated lapilli beds. The pillows/pseudonodules are underlined on the right by a ca. 10 cm thick, massive, ash-dominated contour with a diffuse front to the undisturbed cross-stratified bedsets (mA and dxstA in Fig. 4i). The massive fore front is interpreted as representing the final escape of water that was less coupled with sediments. The liquefaction event is related to a large block impact that could have bounced and compacted the concave central depression. The extreme right of the structure containing stoss stratification dipping at more than the repose angle (upper part of Fig. 4h) may have been oversteepened by the rearrangement of the underlying sediment, a process readily evidenced by Nocita (1988). The coarse lag breccia on top of the central depression may either indicate that the impacting block stayed in place and acted upon the depositional dynamics, resuspended fines during impact, or be a simple infill of the topography.

3.3.2 A trigger for "chute and pool" structures

The two impact SSDs from Laacher See share remarkable similarities with the basal oversteepened truncations observed in structures generally interpreted as "chute and pools" (types I to IV of Schmincke et al., 1973). If the disturbed beds had been slightly more destabilized and permitted entrainment, the same configuration would be observed. Such impact SSDs would explain the oversteepened truncations and be at the origin of some of the "chute and pools" structures (see also Nocita, 1988). This would also explain the observation by Schmincke et al. (1973) that "chute and pools" occur in rather proximal parts, since ballistic blocks are likely to land closer to the crater than the total distance travelled by a PDC. This interpretation does not contradict the subsequent hydraulic jump dynamics of the structures, but the jump would be a consequence of the bed morphology rather than the other way round as usually suggested. A hydraulic jump would however not be necessary and simple morphological blocking of the bedload equally well explains the "chute and pools" depositional patterns (basal blocking and stop-and-go models in Douillet et al., 2013a; Martínez et al., 2007, resp.). The answer likely lies upstream from these structures, at the proximal truncation limit.

3.4 Deformation driven by shock waves

At Tower Hill (Fig. 5), the regularity of patterns, high degree of preservation and absence of slope appear to discredit slumping. The lateral persistence indicates a large-scale effect and discredit shear instabilities. Indeed, a flow with thin granular BBL forming pseudo Kelvin–Helmholtz instabilities is unlikely to stay in this state over several hundred m. Moreover, either lateral flow velocities were slow enough for fine ash and volcanic dust with ripple lamination to deposit, or the ground was covered with a stretch of water. During the phreatomagmatic phase with efficient fragmentation associated with the fine beds, shock waves may have been produced by the explosions (e.g., Scolamacchia and Schouwenaars, 2009). These could propagate close to the rim, quaquaversal to the southern vent, and destabilize the fine-grained bedsets by transmitting their orientation to the ground. Valentine et al. (1989) suggested shock waves as a possible trigger for overturned flame-like structures. They noted that "when a shock passes over a granular deposit, bed particles experience a lift force due to the change in velocity across the shock" and "the bed immediately behind the shock has been observed in experiments to take on a wavelike configuration" citing the convincing experiments by Borisov et al. (1967). Recent shock experiments by Wayne et al. (2013) developed recumbent vortex-like shapes on dust beds and further support the interpretation (see also Fedorov, 2004).

The Purrumbete structure (Fig. 6) has a preferential direction away from crater: (1) all beds are overturned outside of the crater, (2) the deformation, vorticity degree and thickness of beds involved increase away from crater, whereas (3) the crater-parallel face is chaotic. Microfaults suggest cohesion, and there is neither evidence of traction nor of granular flow in the overlying planar deposits related to fallout, thus granular shear is excluded. An envisaged interpretation is that these beds are involved in a small-scale slump. However, overlying beds lie conformably on top of the deformed strata, and are thus emplaced after deformation, implying that a very small amount of material would have slumped, unlikely to be sufficient to yield a consequent gravita-

SED
6, 3261–3302, 2014

tional potential for deformation. Moreover, the bed is only gently sloping ($< 5^{\circ}$). The overturn, vorticity direction as well as the imbrication fabric at thrust faults would suggest an outward oriented slump, but no scar is visible at the deformation onset (left part). Rather, the evolution of intensity of deformation, absence of scar in the proximal side, and imbrication suggest that deformation could origin from the distal part, with some force pushing the sediment toward the crater. Similarly as for the Tower Hill maar, these structures can be the record of shock waves that destabilized the uppermost deposits and transferred them a tilt. Here again, the vortex-like entrainment evidenced in shock experiments supports the interpretation (Borisov et al., 1967; Wayne et al., 2013), and the proximity from the vent make shock wave influence probable. The passage of a shock wave is likely asedimentary (not associated with deposition), and the conformity of overlying fall beds supports a trigger mechanism without sedimentation, the signature being uniquely present as deformation. As SSD triggered by shock waves, these can share similarities with Richtmyer-Meshkov instabilities (Brouillette, 2002).

4 Conclusions

The exercise presented here has demonstrated the richness of information contained in SSD structures from the dilute PDC environment. SSD contains a record of syn-flow and syn-eruptive processes combined with post-depositional bed-state information.

Syn-flow processes were evidenced through granular, pseudo Kelvin–Helmholtz instabilities as well as evidences of suction and injection related to dynamic pore pressure of the flows. These observations feed the understanding of BBL processes of PDCs. Basal intrusions support the interpretation of fluidized flows with dynamic pore overpressure. Vortex-shaped laminae may be a valid indicator of granular-based flows or traction carpets. The suction vs. injection at the base of flows can relate to depletive resp. accumulative phases of a flow.

SED
6, 3261–3302, 2014

Several syn-eruptive processes are recorded by SSD. Ballistic impacts may take more evolved forms than simple sags. They yield information on the bed state such as the compaction degree and water content, which helps to delimit eruptive units and environmental context. Some forms of impact may be at the origin of the so-called "chute and pools" bedforms. Slumps similarly inform on water content and eruptive units. The understanding of prevailing eruption type (wet vs. dry eruptions) may thus benefit from thorough analysis of SSD. Finally, we suggest that shock waves may leave a signature in the sediments by destabilization and overturning of the surface beds close to the vent without any direct deposits.

SSD from PDCs are of interest in the context of sedimentary research since they record subaerial, syn- and post-flow SSD structures, emphasizing that water is not a prerequisite for SSD. Moreover, PDC deposits can be unstable and have large permeability contrasts that facilitate SSD formation. Finally, the recognition of structures similar to instabilities occurring at fluid boundaries (Kelvin–Helmholz, Rayleigh–Taylor) further emphasizes the similarities between fluids and granular mixtures. SSD seems widespread in deposits of dilute PDCs, especially from phreatomagmatic eruptions, and should be addressed more attention. The variety of possible triggers, especially in the context of explosive volcanic eruptions, calls for further field and experimental work.

Appendix A: Instabilities between two fluids

A1 Granular Kelvin–Helmholtz instabilities at a bed-flow interface

Given structures interpreted as granular Kelvin–Helmholtz instabilities, a theoretical resolution similar to the fluid instability can be expressed (Rowley et al., 2011). Any fluid dynamics analysis is based on the integration of "infinitesimal fluid elements", a notion comparable to grains in a granular mixture. The fluid-dynamics analytical method just justify in itself its applicability to granular mediums.

SED
6, 3261–3302, 2014

The problem is taken in 2-D with reference frame ($\boldsymbol{e}_x$ -flow parallel direction-, $\boldsymbol{e}_z$ -upward direction parallel to $\boldsymbol{g}$, the gravity acceleration-). Consider two homogenous mediums F_1 and F_2, F_2 lying above F_1 and the interface an infinite horizontal plane. Suppose the fluids of densities ρ_1 and ρ_2, incompressible ($D\rho_{1,2}/Dt = 0$), inviscid ($\nu = 0$), with constant horizontal velocity $u_{1,2}(z) = U_{1,2}\boldsymbol{e}_x$ and irrotational. The surface disturbance (ξ) can be written in the form (see Drazin, 2002; Douillet, 2014, Chap. 2):

$$\xi = \widetilde{\xi}\exp(i(kx) - st) \tag{A1}$$

with k the wave number. Linearization of the problem posed by the boundary conditions has solution (see Drazin, 2002; Douillet, 2014, Chap. II.2):

$$s = ik\frac{\rho_1 U_1 + \rho_2 U_2}{\rho_1 + \rho_2} \pm \left[\frac{k^2\rho_1\rho_2(U_1 - U_2)^2}{(\rho_1 + \rho_2)^2} - \frac{kg(\rho_1 - \rho_2)}{\rho_1 + \rho_2}\right]^{1/2} \tag{A2}$$

Assumptions can be made for the case of an instability between a granular flow and deposit. The deposit does not move ($U_1 = 0$) and the flow density is a portion of the deposit density ($\rho_2 = x\rho_1$ with $0 \le x \le 1$). Thus Eq. (A2) simplifies into:

$$s = ikU_2\frac{x}{1 + x} \pm \left[k^2U_2^2\frac{x}{(1 + x)^2} - kg\frac{(1 - x)}{(1 + x)}\right]^{1/2} \tag{A3}$$

In order that a wave occurs, Eq. (A3) must have an imaginary component (the angular velocity $w = \mathrm{Im}(s)$). The second term in s must be real for an exponential decay or increase to develop, and thus, be an *instability*. Thus the term under the square root must be positive and a condition for a bed-flow instability is (see also Rowley et al., 2011):

$$U_2^2 > \frac{g}{k}\frac{(1 - x^2)}{x} \tag{A4}$$

This condition is granted for large wavenumber (k), i.e. short waves, high particle concentrations (x), or large flow velocities (Fig. 8).

Further, the phase velocity of an instability ($c = w/k$) can be derived:

$$c = \frac{x}{1+x} U_2 \tag{A5}$$

Under the assumptions, the wave velocity is thus entirely characterized by the concentration difference between the bed and flow (x) and the velocity of the latter (U_2), and the wavelength of the instability ($\lambda = 2\pi/k$) does not appear explicitly.

A2 Granular Rayleigh–Taylor instabilities

A Rayleigh–Taylor instability is a surface instability between two resting fluids of different densities. Thus Eq. (A2) can be equally used with $U_{1,2} = 0$. For the case of the curled and pulled appart structures at Ubehebe (Fig. 1b), the upper coarse grained layer was sinking in the massive fine-grained layer underneath, thus $\rho_2 = x\rho_1$ with $x \geq 1$, and Eq. (A2) simplifies into:

$$s = \pm \left[kg \frac{|1-x|}{1+x} \right]^{1/2} \tag{A6}$$

The field observation is the lengthscale of the curled layers ($\lambda = 2\pi/k =$ ca. 15–30 cm). The missing variables are a timescale for the growth of the instability and the density ratio. Estimating one permits to quantify the other.

Acknowledgements. We are indebted to the following (partial) funding sources: the Bavarian grant THESIS (GAD), the German Deutsche Forschungsgemeinschaft grant KU2689/2-1 (GAD and UK), a Research Professorship (LMUexcellent) of the Bundesexzellenzinitiative and an advanced grant from the European Research Council-EVOKES (DBD).

References

Allen, J. and Banks, N.: An interpretation and analysis of recumbent-folded deformed cross-bedding, Sedimentology, 19, 257–283, 1972. 3265, 3268

Alsop, G. and Marco, S.: Soft-sediment deformation within seismogenic slumps of the Dead Sea Basin, J. Struct. Geol., 33, 433–457, 2011. 3265

Alsop, G. I. and Marco, S.: Tsunami and seiche-triggered deformation within offshore sediments, Sediment. Geol., 261, 90–107, 2012. 3264

Andrews, G. D. and Branney, M. J.: Emplacement and rheomorphic deformation of a large, lava-like rhyolitic ignimbrite: Grey's Landing, southern Idaho, Geol. Soc. Am. Bull., 123, 725–743, 2011. 3266

Bernard, J., Kelfoun, K., Le Pennec, J.-L., and Vargas, S. V.: Pyroclastic flow erosion and bulking processes: comparing field-based vs. modeling results at Tungurahua volcano, Ecuador, B. Volcanol., 76, 1–16, 2014. 3269, 3277

Borisov, A., Lyubimov, A., Kogarko, S., and Kozenko, V.: Instability of the surface of a granular medium behind sliding shock and detonation waves, Combust. Explo. Shock+, 3, 95–97, 1967. 3280, 3281

Brand, B. D. and Clarke, A. B.: The architecture, eruptive history, and evolution of the Table Rock Complex, Oregon: from a Surtseyan to an energetic maar eruption, J. Volcanol. Geoth. Res., 180, 203–224, 2009. 3266, 3267

Brand, B. D. and White, C. M.: Origin and stratigraphy of phreatomagmatic deposits at the Pleistocene Sinker Butte volcano, western Snake River Plain, Idaho, J. Volcanol. Geoth. Res., 160, 319–339, 2007. 3266, 3267

Branney, M., Barry, T., and Godchaux, M.: Sheathfolds in rheomorphic ignimbrites, B. Volcanol., 66, 485–491, 2004. 3266

Branney, M. J. and Kokelaar, B. P.: Pyroclastic density currents and the sedimentation of ignimbrites, Geo. Soc. Mem., 27, 143 pp., 2002. 3266, 3267

Branney, M. J. and Kokelaar, P.: Volcanotectonic faulting, soft-state deformation, and rheomorphism of tuffs during development of a piecemeal caldera, English Lake District, Geol. Soc. Am. Bull., 106, 507–530, 1994. 3266, 3267

Bridge, J. and Demicco, R.: Earth Surface Processes, Landforms and Sediment Deposits, Cambridge University Press, 2008. 3265, 3274

SED

6, 3261–3302, 2014

Soft-sediment deformation of PDC deposits

G. A. Douillet et al.

Brouillette, M.: The Richtmyer–Meshkov instability, Annu. Rev. Fluid Mech., 34, 445–468, 2002. 3281
Brown, R. J., Orsi, G., and de Vita, S.: New insights into Late Pleistocene explosive volcanic activity and caldera formation on Ischia (southern Italy), B. Volcanol., 70, 583–603, 2008. 3267
Caicedo-Carvajal, C. E., Glasser, B. J., and Shinbrot, T.: Granular flow transitions on sinusoidal surfaces, J. Fluid Mech., 556, 253–269, 2006. 3268
Chan, M. A. and Bruhn, R. L.: Dynamic liquefaction of Jurassic sand dunes: processes, origins, and implications, Earth Surf. Proc. Land., 39, 1478–1491, 2014. 3277
Charbonnier, S. J. and Gertisser, R.: Field observations and surface characteristics of pristine block-and-ash flow deposits from the 2006 eruption of Merapi Volcano, Java, Indonesia, J. Volcanol. Geoth. Res., 177, 971–982, 2008. 3267
Chen, J. and Lee, H. S.: Soft-sediment deformation structures in Cambrian siliciclastic and carbonate storm deposits (Shandong Province, China): differential liquefaction and fluidization triggered by storm-wave loading, Sediment. Geol., 288, 81–94, 2013. 3264
Conway, S. L., Shinbrot, T., and Glasser, B. J.: A Taylor vortex analogy in granular flows, Nature, 431, 433–437, 2004. 3268
Crowe, B. M. and Fisher, R. V.: Sedimentary structures in base-surge deposits with special reference to cross-bedding, Ubehebe Craters, Death Valley, California, Geol. Soc. Am. Bull., 84, 663–682, 1973. 3264, 3267, 3269
Denis, M., Guiraud, M., Konaté, M., and Buoncristiani, J.-F.: Subglacial deformation and water-pressure cycles as a key for understanding ice stream dynamics: evidence from the Late Ordovician succession of the Djado Basin (Niger), Int. J. Earth Sci., 99, 1399–1425, 2010. 3264
Doronzo, D. M. and Dellino, P.: Pyroclastic density currents and local topography as seen with the conveyer model, J. Volcanol. Geoth. Res., 278, 25–39, 2014. 3266
Douillet, G., Ghienne, J.-F., Géraud, Y., Abueladas, A., Diraison, M., and Al-Zoubi, A.: Late Ordovician tunnel valleys in southern Jordan, Geol. Soc. Sp., 368, 275–292, 2012. 3264, 3276
Douillet, G. A.: Flow and sedimentation from pyroclastic density currents. From large scale to boundary layer processes, Ph.D. thesis, October 2014, Earth and Environmental Sciences, Ludwig Maximilian University, 2014. 3283

SED
6, 3261–3302, 2014

Douillet, G. A., Pacheco, D. A., Kueppers, U., Letort, J., Tsang-Hin-Sun, È., Bustillos, J., Hall, M., Ramón, P., and Dingwell, D. B.: Dune bedforms produced by dilute pyroclastic density currents from the August 2006 eruption of Tungurahua volcano, Ecuador, B. Volcanol., 75, 1–20, 2013a. 3270, 3279

Douillet, G. A., Tsang-Hin-Sun, È., Kueppers, U., Letort, J., Pacheco, D. A., Goldstein, F., Von Aulock, F., Lavallée, Y., Hanson, J. B., Bustillos, J., Robin, C., Ramón, P., Hall, M., and Dingwell, D. B.: Sedimentology and geomorphology of the deposits from the August 2006 pyroclastic density currents at Tungurahua volcano, Ecuador, B. Volcanol., 75, 1–21, 2013b. 3270

Douillet, G. A., Rasmussen, K. R., Kueppers, U., Lo Castro, D., Merrison, J. P., Iversen, J. J., and Dingwell, D. B.: Saltation threshold for pyroclasts at various bedslopes: wind tunnel measurements, J. Volcanol. Geoth. Res., 278, 14–24, 2014. 3266, 3274

Drazin, P. G.: Introduction to Hydrodynamic Stability, Cambridge University Press, 2002. 3283

Ettensohn, F., Zhang, C., Gao, L., and Lierman, R.: Soft-sediment deformation in epicontinental carbonates as evidence of paleoseismicity with evidence for a possible new seismogenic indicator: accordion folds, Sediment. Geol., 235, 222–233, 2011. 3264

Farin, M., Mangeney, A., and Roche, O.: Fundamental changes of granular flow dynamics, deposition, and erosion processes at high slope angles: insights from laboratory experiments, J. Geophys. Res.-Earth, 119, 504–532, 2014. 3268, 3274, 3277

Fedorov, A.: Mixing in wave processes propagating in gas mixtures (review), Combust. Explo. Shock+, 40, 17–31, 2004. 3280

Fiske, R. S.: Subaqueous pyroclastic flows in the Ohanapecosh Formation, Washington, Geol. Soc. Am. Bull., 74, 391–406, 1963. 3266

Fiske, R. S. and Tobisch, O. T.: Paleogeographic significance of volcanic rocks of the Ritter Range pendant, central Sierra Nevada, California, Pacific Coast Paleogeography Symposium 2: Mesozoic Paleogeography of the Western United States, 391–406, 1978. 3267

Forterre, Y. and Pouliquen, O.: Longitudinal vortices in granular flows, Phys. Rev. Lett., 86, 5886–5889, 2001. 3268

Gençalioğlu-Kuşcu, G., Atilla, C., Cas, R. A., and Kuşcu, İ.: Base surge deposits, eruption history, and depositional processes of a wet phreatomagmatic volcano in Central Anatolia (Cora Maar), J. Volcanol. Geoth. Res., 159, 198–209, 2007. 3267

SED
6, 3261–3302, 2014

Soft-sediment deformation of PDC deposits

G. A. Douillet et al.

Gernon, T., Fontana, G., Field, M., Sparks, R., Brown, R., and Mac Niocaill, C.: Pyroclastic flow deposits from a kimberlite eruption: the Orapa South Crater, Botswana, Lithos, 112, 566–578, 2009. 3267

Gernon, T. M., Sparks, R. S. J., and Field, M.: Degassing structures in volcaniclastic kimberlite: examples from southern African kimberlite pipes, J. Volcanol. Geoth. Res., 174, 186–194, 2008. 3267

Ghienne, J.-F.: Late Ordovician sedimentary environments, glacial cycles, and post-glacial transgression in the Taoudeni Basin, West Africa, Palaeogeogr. Palaeocl., 189, 117–145, 2003. 3264

Giannetti, B. and Luongo, G.: Trachyandesite scoria-flow and associated trachyte pyroclastic flow and surge at Roccamonfina Volcano (Roman Region, Italy), J. Volcanol. Geoth. Res., 59, 313–334, 1994. 3267, 3276

Gibert, L., Alfaro, P., García-Tortosa, F., and Scott, G.: Superposed deformed beds produced by single earthquakes (Tecopa Basin, California): insights into paleoseismology, Sediment. Geol., 235, 148–159, 2011. 3264, 3267, 3273

Goldfarb, D. J., Glasser, B. J., and Shinbrot, T.: Shear instabilities in granular flows, Nature, 415, 302–305, 2002. 3268

Hall, M. L., Steele, A. L., Mothes, P. A., and Ruiz, M. C.: Pyroclastic density currents (PDC) of the 16–17 August 2006 eruptions of Tungurahua volcano, Ecuador: geophysical registry and characteristics, J. Volcanol. Geoth. Res., 265, 78–93, 2013. 3269

Jordan, S., Cas, R., and Hayman, P.: The origin of a large (> 3 km) maar volcano by coalescence of multiple shallow craters: Lake Purrumbete maar, southeastern Australia, J. Volcanol. Geoth. Res., 254, 5–22, 2013. 3266, 3267, 3272

Kelfoun, K., Samaniego, P., Palacios, P., and Barba, D.: Testing the suitability of frictional behaviour for pyroclastic flow simulation by comparison with a well-constrained eruption at Tungurahua volcano (Ecuador), B. Volcanol., 71, 1057–1075, 2009. 3269

Komorowski, J.-C., Jenkins, S., Baxter, P. J., Picquout, A., Lavigne, F., Charbonnier, S., Gertisser, R., Preece, K., Cholik, N., Budi-Santoso, A., and Surono: Paroxysmal dome explosion during the Merapi 2010 eruption: processes and facies relationships of associated high-energy pyroclastic density currents, J. Volcanol. Geoth. Res., 261, 260–294, 2013. 3267, 3276

Leclair, S. F. and Arnott, R. W. C.: Parallel lamination formed by high-density turbidity currents, J. Sediment. Res., 75, 1–5, 2005. 3275

SED
6, 3261–3302, 2014
Soft-sediment deformation of PDC deposits
G. A. Douillet et al.

Lowe, D. R.: Water escape structures in coarse-grained sediments, Sedimentology, 22, 157–204, 1975. 3264

Mangeney, A., Roche, O., Hungr, O., Mangold, N., Faccanoni, G., and Lucas, A.: Erosion and mobility in granular collapse over sloping beds, J. Geophys. Res.-Earth, 115, doi:10.1029/2009JF001462, 2010. 3268

Martínez, E., Pérez-Penichet, C., Sotolongo-Costa, O., Ramos, O., Måløy, K., Douady, S., and Altshuler, E.: Uphill solitary waves in granular flows, Phys. Rev. E, 75, 031303, doi:10.1103/PhysRevE.75.031303, 2007. 3279

Mattsson, H. B. and Tripoli, B. A.: Depositional characteristics and volcanic landforms in the Lake Natron–Engaruka monogenetic field, northern Tanzania, J. Volcanol. Geoth. Res., 203, 23–34, 2011. 3267

McDonough, W. F., Waibel, A. F., and Gannet, M. W.: The re-interpretation of the Leone Lake sediments as a pyroclastic surge deposit and its tectonic significance, J. Volcanol. Geoth. Res., 20, 101–115, 1984. 3267

Mills, P. C.: Genesis and diagnostic value of soft-sediment deformation structures – a review, Sediment. Geol., 35, 83–104, 1983. 3264, 3265, 3268, 3269, 3273, 3274

Mohindra, R. and Bagati, T.: Seismically induced soft-sediment deformation structures (seismites) around Sumdo in the lower Spiti valley (Tethys Himalaya), Sediment. Geol., 101, 69–83, 1996. 3264

Niebling, M. J., Flekkøy, E. G., Måløy, K. J., and Toussaint, R.: Sedimentation instabilities: impact of the fluid compressibility and viscosity, Phys. Rev. E, 82, 051302, doi:10.1103/PhysRevE.82.051302, 2010. 3264, 3273

Nocita, B. W.: Soft-sediment deformation (fluid escape) features in a coarse-grained pyroclastic-surge deposit, north-central New Mexico, Sedimentology, 35, 275–285, 1988. 3267, 3279

Odonne, F., Callot, P., Debroas, E.-J., Sempere, T., Hoareau, G., and Maillard, A.: Soft-sediment deformation from submarine sliding: favourable conditions and triggering mechanisms in examples from the Eocene Sobrarbe delta (Ainsa, Spanish Pyrenees) and the mid-Cretaceous Ayabacas Formation (Andes of Peru), Sediment. Geol., 235, 234–248, 2011. 3265

Owen, G.: Deformation processes in unconsolidated sands, Geol. Soc. Sp., 29, 11–24, 1987. 3264

Owen, G.: Experimental soft-sediment deformation: structures formed by the liquefaction of unconsolidated sands and some ancient examples, Sedimentology, 43, 279–293, 1996. 3264, 3273

SED
6, 3261–3302, 2014
Soft-sediment deformation of PDC deposits
G. A. Douillet et al.

Owen, G.: Load structures: gravity-driven sediment mobilization in the shallow subsurface, Geol. Soc. Sp., 216, 21–34, 2003. 3264
Owen, G. and Moretti, M.: Determining the origin of soft-sediment deformation structures: a case study from Upper Carboniferous delta deposits in south-west Wales, UK, Terra Nova, 20, 237–245, 2008. 3264
Owen, G., Moretti, M., and Alfaro, P.: Recognising triggers for soft-sediment deformation: current understanding and future directions, Sediment. Geol., 235, 133–140, 2011. 3264
Peltier, A., Finizola, A., Douillet, G. A., Brothelande, E., and Garaebiti, E.: Structure of an active volcano associated with a resurgent block inferred from thermal mapping: the Yasur–Yenkahe volcanic complex (Vanuatu), J. Volcanol. Geoth. Res., 243, 59–68, 2012. 3273
Pisarska-Jamroży, M. and Weckwerth, P.: Soft-sediment deformation structures in a Pleistocene glaciolacustrine delta and their implications for the recognition of subenvironments in delta deposits, Sedimentology, 60, 637–665, 2013. 3264
Pistolesi, M., Delle Donne, D., Pioli, L., Rosi, M., and Ripepe, M.: The 15 March 2007 explosive crisis at Stromboli volcano, Italy: assessing physical parameters through a multidisciplinary approach, J. Geophys. Res.-Sol. Ea., 116, doi:10.1029/2011JB008527, 2011. 3267
Prata, G.: Complex Eruption Style and Deposit Changes During the Evolution of the Late Pleistocene Tower Hill Maar-scoria Cone Volcanic Complex, Newer Volcanics Province, Victoria, Australia, Monash University Melbourne, 2012. 3272
Prata, G. and Cas, R.: Cyclicity in Fluctuating Phreatomagmatic and Magmatic Eruptive Styles at the 35 ka Tower Hill Volcanic Complex, Southeast Australia, Geoscience Society of New Zealand Miscellaneous Publication 131A, p. 136, 2012. 3271
Rawcliffe, H. J. and Brown, D. J.: Lithofacies architecture of basaltic andesite lavas and their interaction with wet-sediment: Part A – Chroinn, Kerrera, NW Scotland, Scot. J. Geol., 50, 49–55, 2014. 3266
Roche, O., Nĩno, Y., Mangeney, A., Brand, B., Pollock, N., and Valentine, G. A.: Dynamic pore-pressure variations induce substrate erosion by pyroclastic flows, Geology, 41, 1170–1110, 2013. 3268, 3273, 3274, 3277
Røe, S.-L., and Hermansen, M.: New aspects of deformed cross-strata in fluvial sandstones: examples from Neoproterozoic formations in northern Norway, Sediment. Geol., 186, 283–293, 2006. 3265, 3268
Rowley, P. J.: Analogue modelling of pyroclastic density current deposition, Royal Holloway, University of London, Unpublished Ph.D. thesis, 2010. 3267, 3268

Rowley, P. J., Kokelaar, P., Menzies, M., and Waltham, D.: Shear-derived mixing in dense granular flows, J. Sediment. Res., 81, 874–884, 2011. 3265, 3267, 3268, 3274, 3275, 3276, 3282, 3283
Sasnett, P., Goehring, B. M., Christie-Blick, N., and Schaefer, J. M.: Do phreatomagmatic eruptions at Ubehebe Crater (Death Valley, California) relate to a wetter than present hydroclimate?, Geophys. Res. Lett., 39, doi:10.1029/2011GL050130, 2012. 3269
Schmincke, H.-U., Fisher, R. V., and Waters, A. C.: Antidune and chute and pool structures in the base surge deposits of the Laacher See area, Germany, Sedimentology, 20, 553–574, 1973. 3271, 3279, 3301
Scolamacchia, T. and Schouwenaars, R.: High-speed impacts by ash particles in the 1982 eruption of El Chichon, Mexico, J. Geophys. Res.-Sol. Ea., 114, doi:10.1029/2008JB005848, 2009. 3280
Selker, J. S.: Expressions for the formation of load casts in soft sediment, J. Sediment. Res., 63, 1149–1151, 1993. 3274
Sherwood, J., Oyston, B., and Kershaw, A.: The age and contemporary environments of Tower Volcano, Southwest Victoria, Australia, Proceedings of the Royal Society of Victoria, 116, 69–76, 2004. 3271
Smith, N. J. and Kokelaar, B. P.: Proximal record of the 273 ka Poris caldera-forming eruption, Las Cañadas, Tenerife, B. Volcanol., 75, 1–21, 2013. 3267
Stinton, A. J., Cole, P. D., Stewart, R. C., Odbert, H. M., and Smith, P.: The 11 February 2010 partial dome collapse at Soufrière Hills Volcano, Montserrat, Geo. Soc. Mem., 39, 133–152, 2014. 3270, 3276
Sulpizio, R. and Dellino, P.: Sedimentology, depositional mechanisms and pulsating behaviour of pyroclastic density currents, Dev. Volcano., 10, 57–96, 2008. 3266
Valentine, G. A., Buesch, D. C., and Fisher, R. V.: Basal layered deposits of the Peach Springs Tuff, northwestern Arizona, USA, B. Volcanol., 51, 395–414, 1989. 3267, 3268, 3280
Van Loon, A.: Soft-sediment deformation structures in siliciclastic sediments: an overview, Geologos, 15, 3–55, 2009. 3264
Vazquez, J. A. and Ort, M. H.: Facies variation of eruption units produced by the passage of single pyroclastic surge currents, Hopi Buttes volcanic field, USA, J. Volcanol. Geoth. Res., 154, 222–236, 2006. 3266

Vinningland, J. L., Johnsen, Ø., Flekkøy, E. G., Toussaint, R., and Måløy, K. J.: Granular rayleigh-taylor instability: experiments and simulations, Phys. Rev. Lett., 99, 1149–1151, 2007. 3274

Vinningland, J. L., Johnsen, Ø., Flekkøy, E. G., Toussaint, R., and Måløy, K. J.: Size invariance of the granular Rayleigh–Taylor instability, Phys. Rev. E, 81, 041308, doi:10.1103/PhysRevE.81.041308, 2010. 3274

Voight, B., Janda, R., and Douglass, P.: Nature and mechanics of the Mount St Helens rockslide-avalanche of 18 May 1980, Geotechnique, 33, 243–273, 1983. 3267

Wadge, G., Robertson, R., and Voight, B.: The Eruption of Soufriere Hills Volcano, Montserrat from 2000 to 2010, Geological Society of London, 2014. 3270

Ward, S. N. and Day, S.: Particulate kinematic simulations of debris avalanches: interpretation of deposits and landslide seismic signals of Mount Saint Helens, 1980 May 18, Geophys. J. Int., 167, 991–1004, 2006. 3267

Waters, A. C. and Fisher, R. V.: Base surges and their deposits: Capelinhos and Taal volcanoes, J. Geophys. Res., 76, 5596–5614, 1971. 3272

Wayne, P. J., Vorobieff, P., Smyth, H., Bernard, T., Corbin, C., Maloney, A., Conroy, J., White, R., Anderson, M., Kumar, S., Truman, R., and Srivastava, D.: Shock-driven particle transport off smooth and rough surfaces, J. Fluid. Eng.-T. ASME, 135, 061302, doi:10.1115/1.4023786, 2013. 3280, 3281

Whelley, P. L., Jay, J., Calder, E., Pritchard, M., Cassidy, N., Alcaraz, S., and Pavez, A.: Post-depositional fracturing and subsidence of pumice flow deposits: Lascar Volcano, Chile, B. Volcanol., 74, 511–531, 2012. 3267

Wiemer, G.: On the Role of volcanic ash in submarine landslide initiation processes, Ph.D. thesis, Fachbereich Geowissenschaften der Universität Bremen, Bremen, 2014. 3273

SED

6, 3261–3302, 2014

Soft-sediment deformation of PDC deposits

G. A. Douillet et al.

Table 1. Main characteristics of SSD structures presented in figures and discussed in text. Abbreviations: F-F: folds-and-faults; PN: pseudonodules; D:dikes; P: pipes; DFL: diapiric-flame-like; OB/L: overturned bed/lamination; VB/L: vortex bed/lamination; OsL: oversteepened.

Location	Figure	SSD type	Description	Dimensions	SSD orientation	Involved beds	Underlying beds	Overlying beds	Water	Interpretation
Ubehebe	1a, c	F-F	Stack of angular folds imbricated by small thrust faults	Involved beds ca. 20 cm thick and 50 cm between faults	Toward a channel thalweg	ca. 20 cm thick succession of massive fine ash, planar laminated fine ash, coarse ash, and planar laminated fine ash	Massive ash with deformed lenses of the remnants of a coarser horizon	Apparently massive fine ash and volcanic dust. Produce small scale SSD at the contact	Likely	Slump fold during channel re-opening; wet sediment
Ubehebe	1b	Curled, isolated PN	Curled and isolated layers of coarse ash	30–50 cm long layers, few cms thick	No orientation	Layers of planar ash/coarse ash with local small scale DFL SSD	Massive ash	Massive ash	Likely	Detached PN; granular Rayleigh–Taylor instabilities
Ubehebe	1d top	DFL	Chaotic vertical SSD, possible orientation recumbent with flow	ca. 15 cm amplitude; few cm thick beds	Outcrop sub parallel to a channel	Diffuse planar bedset of ash and underlying massive fine ash	Massive fine ash	Sub-planar cms-thick fine ash overlain by planar, cms-thick coarse ash	Likely	Granular Rayleigh–Taylor instabilities
Ubehebe	1d mid right	OB	Lonely, recumbent tailing anticline	ca. 5 cm thick and long	Outcrop sub parallel to a channel	Boarder between two layers of massive ash	Massive fine ash with clasts (dark)	Massive fine ash (grey)	Possible	Granular shear instability
Ubehebe	1d base	VB	Recumbent shark fin and vortices	5 cm thick and long	Outcrop sub parallel to a channel	Limit between 2 layers	Massive fine ash with clasts (dark)	Massive fine ash with less clasts (lighter)	Possible	Granular Kelvin–Helmholtz instabilities
Ubehebe	1e	PN, D, sag	Impact sag underlain by PN and small D	0–5 cm amplitude PN; 5–10 cm long dikes	Unrelated to flow	Few cm thick massive coarse ash	Massive to faintly planar-stratified ash	Roughly planar-stratified coarse ash laminations	Likely	Impact-induced liquefaction of the porous and water saturated coarse ash
Soufrière Hills	3a, b	P, D, PN, VL	Dark lapilli ash layer concentrating SSD at its boarders	P: 1 cm diam., $< f$10 cm long, PN: 3–8 cm, VL and D: 2–4 cm	P unsheared VL with flow	Dark massive lapilli-ash layer and overlying massive ash layer	Diffusely stratified ash layer	Massive ash and lapilli layer	No	Basal D injections from overpressured fluidized flow and degassing P from deflation after deposition
Soufrière Hills	3c	Depression	Circular depression at the surface	ca. 3 m diam., 10 cm depression	No orientation	Probably whole unit	/	/	Unlikely	Compaction structure by gas escape and grain rearrangement
Tungurahua	2b	OL/VL	Recumbent shark fin	1 cm amplitude, 3 and 5 cm length	Parallel to flow	6 and 7 laminae of ash	Similar ash lamination	Similar ash lamination	No	Granular Kelvin–Helmholtz instability
Tungurahua	2c	OL	Recumbent tailing anticlines	0,8 cm amplitude, 3 cm length	Parallel to flow	7 laminar of ash	Ripple cross-lamination	Similar ash lamination	No	Granular shear instability, possibly Kelvin–Helmholtz instability

SED
6, 3261–3302, 2014

Table 1. Continued.

Location	Figure	SSD type	Description	Dimensions	SSD orientation	Involved beds	Underlying beds	Overlying beds	Water	Interpretation
Laacher See	4a–f	Composite	Tilted blocks/concave beds with DFL/angular F-F	ca. 50–80 cm thick; ca. 5 m long	Roughly outward crater	sequence of faintly bedded ash and lapilli as well as ash beds	lapilli layer overlain by a thin (few cm) layer of ash	Cross-bedded lapilli and ash and 2 impact sags	Possible	Impact of bouncing block
Laacher See	4g–i	Composite	concave beds/PN/OsB	ca. 50–80 cm thick/ca. 3 m long	Roughly outward crater	faintly bedded ash and lapilli	diffuse fore-front of massive ash	lens of large clasts	Possible	Impact of bouncing block with induced liquefaction
Laacher See	4g, h	Lonely anticline	Single upright convex bed (anticline)	15 cm amplitude and length	Sub-parallel to flow	5 cm of otherwise planar bedded ash	Faintly laminated coarse lapilli layer overlain by a massive layer of ash	Cross-bedded lapilli and ash with stoss-depositional dune bedform	Possible	Dynamic or pore pressure driven. Possibly triggered by the presence of overlying dune bedform
Tower Hill	5	In train OsL	Train of slightly OsL/OB beds within ripple cross laminations	ca. 10 cm amplitude; ca. 50 cm wavelength, in train repetitions over 100 s m	Aligned with ripple bedding	ca. 40 cm thick, fine ash bedset, with ripple cross-laminations	Massive, coarse ash fining-up by increasing occurrence of thin sub-planar ash beds	Grading back into massive coarse-ash with reverse sequence	Probable	Shock wave destabilization
Purrumbete	6a, b, e	OL; F-F	Trains of F-F showing VB. Evolution from gentle to plowing SSD	Increase in amplitude and pseudo-wavelength from 5 to 25 cm over 1.5 m	Outward crater	Planar laminated ash bedsets and underlying massive fine ash	Massive, clast rich, fine ash beds	Finely planar-laminated fallout ash	Possible	Shock wave destabilization
Purrumbete	6c, d	DFL	Chaotic DFL SSD	ca. 20 cm amplitude	Perpendicular to rim	Same outcrop	Same outcrop	Same outcrop	Possible	Possible fluid escape

SED
6, 3261–3302, 2014

Soft-sediment deformation of PDC deposits

G. A. Douillet et al.

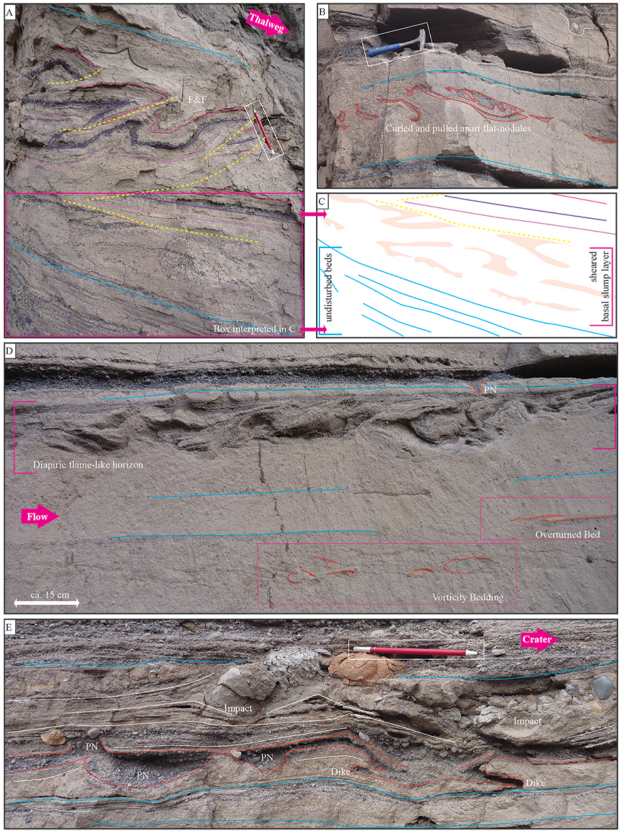

Figure 1. SSD structures from Ubehebe craters. **(a)** folds-and-faults structure (F&F) related to slump, with interpretation of the outlined lower part in **(c)**. **(b)** Curled and pulled apart coarse-grained layers interpreted as detached pseudonodules. **(d)** Diapiric flame-like structures in upper part, recumbent overturned bed in the middle right, vortex beds in the lower part. **(e)** Interpenetrating coarse bed with pseudonodules (PN) and dikes at the base of ballistic impact sags.

SED
6, 3261–3302, 2014

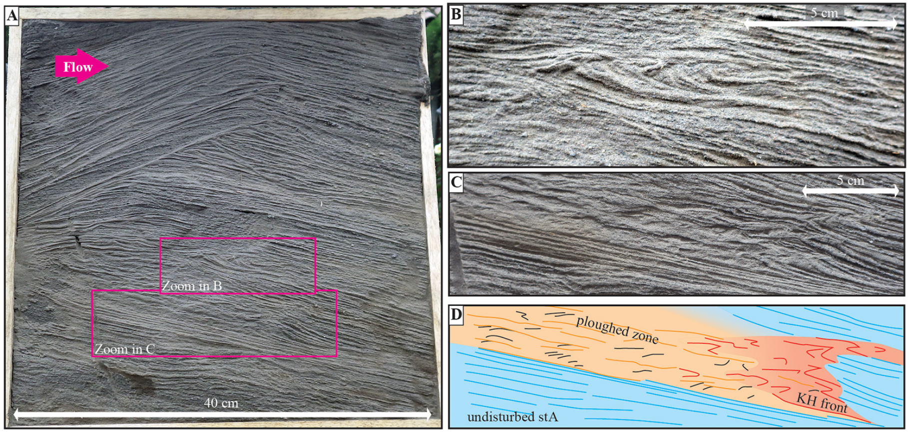

Figure 2. Overturned laminations from Tungurahua in the Achupashal valley illustrating shear in a granular BBL (imprint from lacquer peel). **(a)** peel showing stoss-depositional ash bedsets, insets highlight the borders of **(b)** and **(c)**. **(b)** Imbricated, downflow-recumbent, vortex-shaped SSD structure. **(c)** and **(d)** Recumbent and tailing anticlines form a front of deformation. The zone upstream the front contrasts with the downstream undisturbed bedding: it is comparatively massive, with thick beds and diffuse oversteepened stratification attributed to the ploughing effect of the downstream moving shear instabilities from the deformation front.

SED
6, 3261–3302, 2014

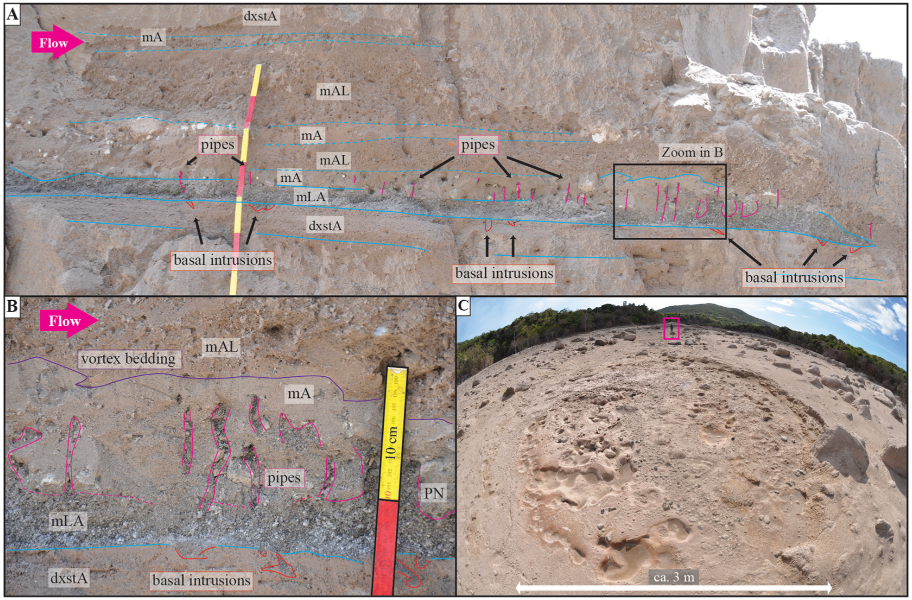

Figure 3. SSD from the 2010 dome collapse PDC deposits at Soufrière Hills in the Belham valley. **(a)** Degassing pipes occur in a massive ash (mA) layer, and seem to emanate from the underlying massive lapilli and ash layer (mLA). The base of the mLA layer also exhibits basal intrusions of small dikes in the underlying diffusely cross-straitified ash bedsets (dxstA). **(b)** Zoom in SSD structures. The upper contact is uneven with a vortex and undulating form. **(c)** Large-scale, circular depression, ca. 10 cm in throw. Note also smaller-scale structures within the main depression.

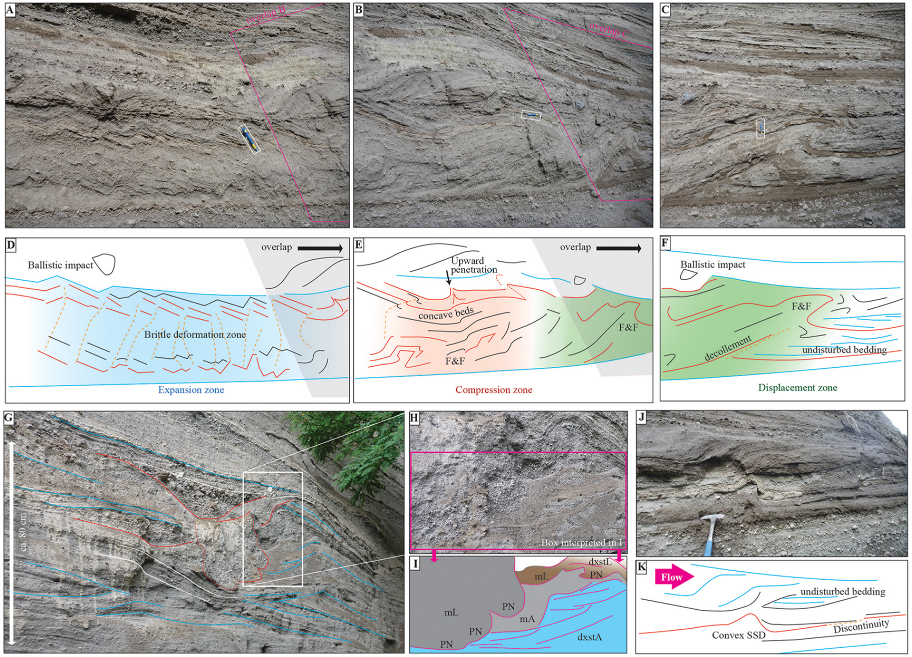

Figure 4. SSD structures from Laacher See. **(a–c)** make a panorama of a composite structure due to impact interpreted in **(d–f)**. Extensional thrust dominos in **(a)**, compression due to impact in **(b)**, and compressional displacement with folds-and-faults in **(c)** (image overlap dashed in grey). **(g–i)** Print of an impact resembling a pseudo "chute and pool". Central compression is topped by lag breccia and rooted by massive lapilli (mL) pseudonodules contoured by massive ash (mA) in otherwise diffusely cross-stratified ash and lapilli (dxstA, dxstL). Zoom in **(h)**, with interpretation in **(i)**. (**j** and **k**): **(a)** solitary symmetrical anticline is contained in a fine grained fall layer and is related to dynamic pore pressure drop by subsequent flows.

SED
6, 3261–3302, 2014

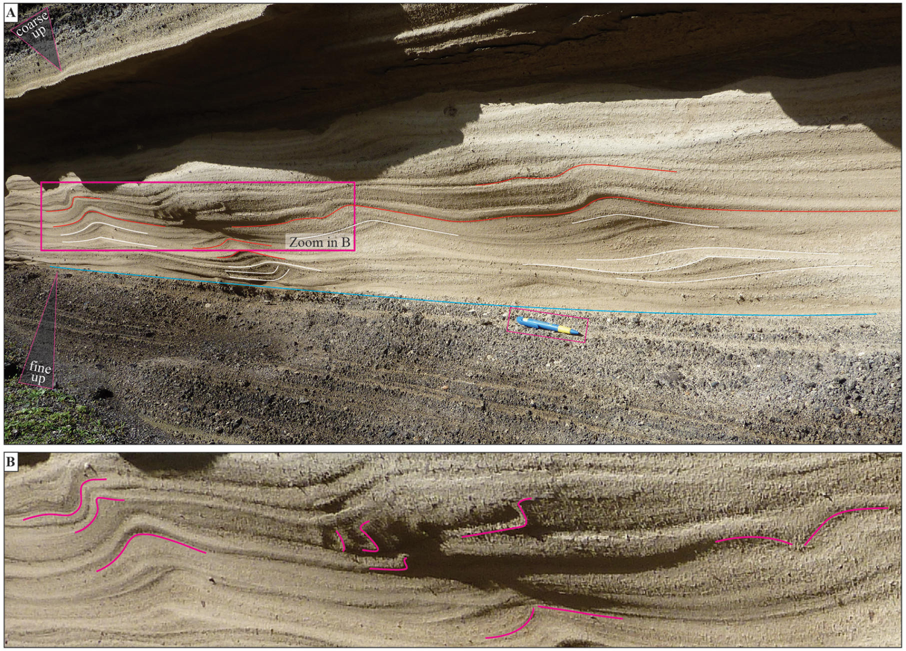

Figure 5. Tower Hill rim: **(a)** Train of slightly overturned and oversteepened laminations in fine ash bedsets with ripple cross-laminations related to shock waves at the vent. Triangles illustrate grading tendencies reflecting a transition from strombolian to phreatomagmatic explosions. **(b)** Zoom in oversteepened and slightly overturned beds.

SED
6, 3261–3302, 2014

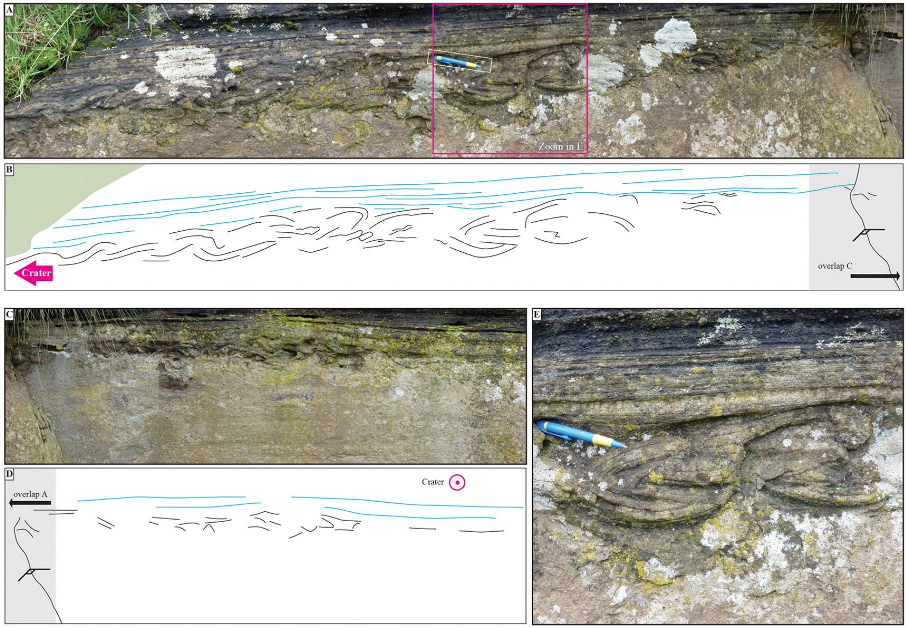

Figure 6. Folds-and-faults in Purrumbete rim. **(a)** Outcrop part oriented outward crater with **(b)** interpretation. Shaded zones indicates the overlap with **(c)**, the outcrop part oriented parallel to rim with **(d)** interpretation. **(e)** Zoom into recumbent folds-and-faults structure with overlying planar lamination (location outlined in **(a)**.

SED
6, 3261–3302, 2014

Soft-sediment deformation of PDC deposits

G. A. Douillet et al.

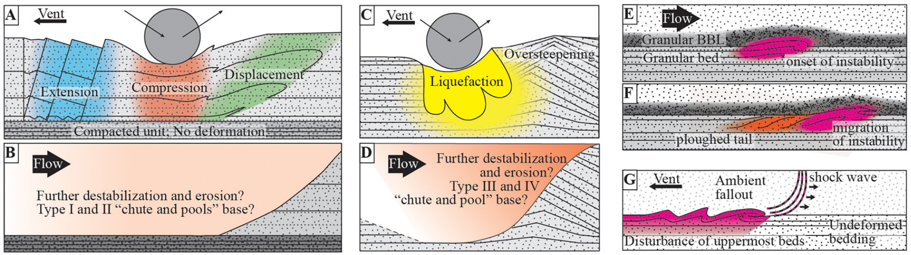

Figure 7. Interpretative sketch of sin-eruptive SSD. **(a)** and **(c)** SSD formed by ballistic impacts. **(b)** and **(d)** Envisaged scenario if destabilization of **(a)** and **(c)** permitted complete remobilization. These would form the base for types I and II “chute and pools” in Schmincke et al. (1973). **(e)** Formation of pseudo Kelvin–Helmholtz instabilities between the bed and basal granular flow, and **(f)** the ploughing effect of a migrating instability. **(g)** Destabilization by shock waves.

SED
6, 3261–3302, 2014

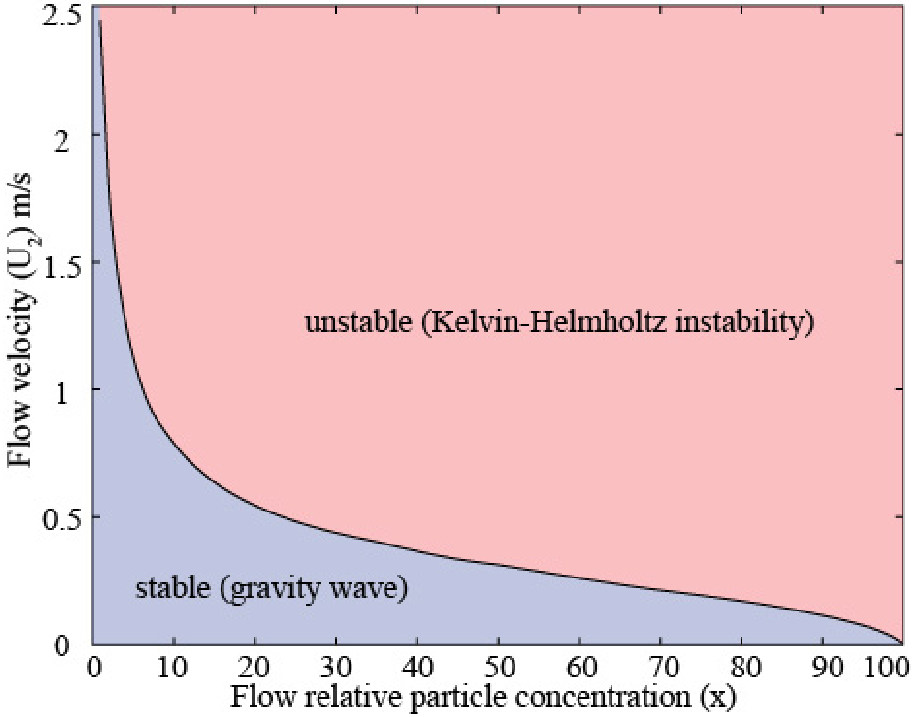

Figure 8. Threshold flow velocity (U_2) as a function of flow's particle concentration compared to bed's particle concentration (x) following Eq. (A4)